AGU PUBLICATIONS

JGR

Journal of Geophysical Research: Oceans

RESEARCH ARTICLE

10.1002/2016JC012676

Indian Ocean sources of Agulhas leakage

Jonathan V. Durgadoo[1], Siren Rühs[1], Arne Biastoch[1], and Claus W. B. Böning[1]

[1]GEOMAR Helmholtz Centre for Ocean Research Kiel, Kiel, Germany

Key Points:
- A study of pathways, timescales, and water transformations of Indian Ocean sources of Agulhas leakage
- On-route, Indonesian Through-Flow cools and salinificates, while Tasman leakage is deeper and experiences no change in properties
- The Pacific contributes at least 7.9 Sv to the total Agulhas leakage of about 14 Sv

Correspondence to:
J. V. Durgadoo,
jdurgadoo@gmail.com

Citation:
Durgadoo, J. V., S. Rühs, A. Biastoch, and C. W. B. Böning (2017), Indian Ocean sources of Agulhas leakage, *J. Geophys. Res. Oceans*, *122*, doi:10.1002/2016JC012676.

Received 30 DEC 2016
Accepted 4 APR 2017
Accepted article online 13 APR 2017

Abstract We examine the mean pathways, transit timescales, and transformation of waters flowing from the Pacific and the marginal seas through the Indian Ocean (IO) on their way toward the South Atlantic within a high-resolution ocean/sea-ice model. The model fields are analyzed from a Lagrangian perspective where water volumes are tracked as they enter the IO. The IO contributes 12.6 Sv to Agulhas leakage, which within the model is 14.1 $\pm$ 2.2 Sv, the rest originates from the South Atlantic. The Indonesian Through-flow constitutes about half of the IO contribution, is surface bound, cools and salinificates as it leaves the basin within 10–30 years. Waters entering the IO south of Australia are at intermediate depths and maintain their temperature-salinity properties as they exit the basin within 15–35 years. Of these waters, the contribution from Tasman leakage is 1.4 Sv. The rest stem from recirculation from the frontal regions of the Southern Ocean. The marginal seas export 1.0 Sv into the Atlantic within 15–40 years, and the waters cool and freshen on-route. However, the model's simulation of waters from the Gulfs of Aden and Oman are too light and hence overly influenced by upper ocean circulations. In the Cape Basin, Agulhas leakage is well mixed. On-route, temperature-salinity transformations occur predominantly in the Arabian Sea and within the greater Agulhas Current region. Overall, the IO exports at least 7.9 Sv from the Pacific to the Atlantic, thereby quantifying the strength of the upper cell of the global conveyor belt.

1. Introduction

In the global ocean circulation, the Indian Ocean (IO) constitutes a connector between the Pacific and Atlantic Oceans. *Broeker*'s [1991] simple but profound schematic of the Great Ocean Conveyor Belt already illustrates the importance of the IO. In the upper ocean, warm tropical waters are imported from the Pacific through the Indonesian Archipelago into the IO and exported south of Africa into the Atlantic where eventually convective overturning occurs at high northern latitudes. The newly formed deep water subsequently spreads southward and is redistributed into the Indian and Pacific Oceans after looping around Antarctica. In this study, we investigate whether the IO simply acts as a passive connector between the Pacific and Atlantic oceans or whether it additionally actively modifies the waters that it communicates across. Since 1991, numerous authors have revised *Broeker*'s depiction, highlighting the complex and eddying nature of both the upper and deep routes [*Richardson*, 2008; *Lozier*, 2010]. Among others, it is now recognized that the route through the IO occurs both north and south of Australia, namely via the Indonesian Through-flow and Tasman leakage (Figure 1).

Water entering the IO from the Indonesian Archipelago, so-called Indonesian Through-flow (ITF), must navigate a complex route. The main entry point from the Pacific Ocean is through Makassar Strait between Borneo and Sulawesi, with over 75% of the ~15 Sv that eventually traverses into the IO [*Sprintall et al*., 2009; *Tillinger and Gordon*, 2009]. The volume transport of ITF displays a relationship with phases of the El-Niño Southern Oscillation. In the negative phase, an enhancement in through-flow has been reported [*Meyers*, 1996; *Liu et al*., 2015], with more waters of south Pacific origin entering Makassar Strait [*van Sebille et al*., 2014]. Further interannual variations in ITF originate from coastal Kelvin waves propagating along the eastern IO basin, and are related to the Indian Ocean Dipole [*Liu et al*., 2015]. Based on 3 decades (since 1984) of repeated expendable bathythermograph measurements between Fremantle (southwest Australia) and Sunda Strait (between the islands of Sumatra and Java) and surface winds measurements, *Wijffels et al*. [2008] and *Liu et al*. [2015] reported a positive trend in geostrophic ITF transport of 1 Sv/decade. ITF waters enter the IO as a tongue of relatively fresh surface waters and saltier intermediate waters [*Gordon et al*., 1997] and feed into the South Equatorial Current. High-resolution numerical experiments with artificial opening and closing of the ITF passages provide evidence of a codependency between ITF transport and Agulhas leakage further downstream [e.g., *Le Bars et al*., 2013].

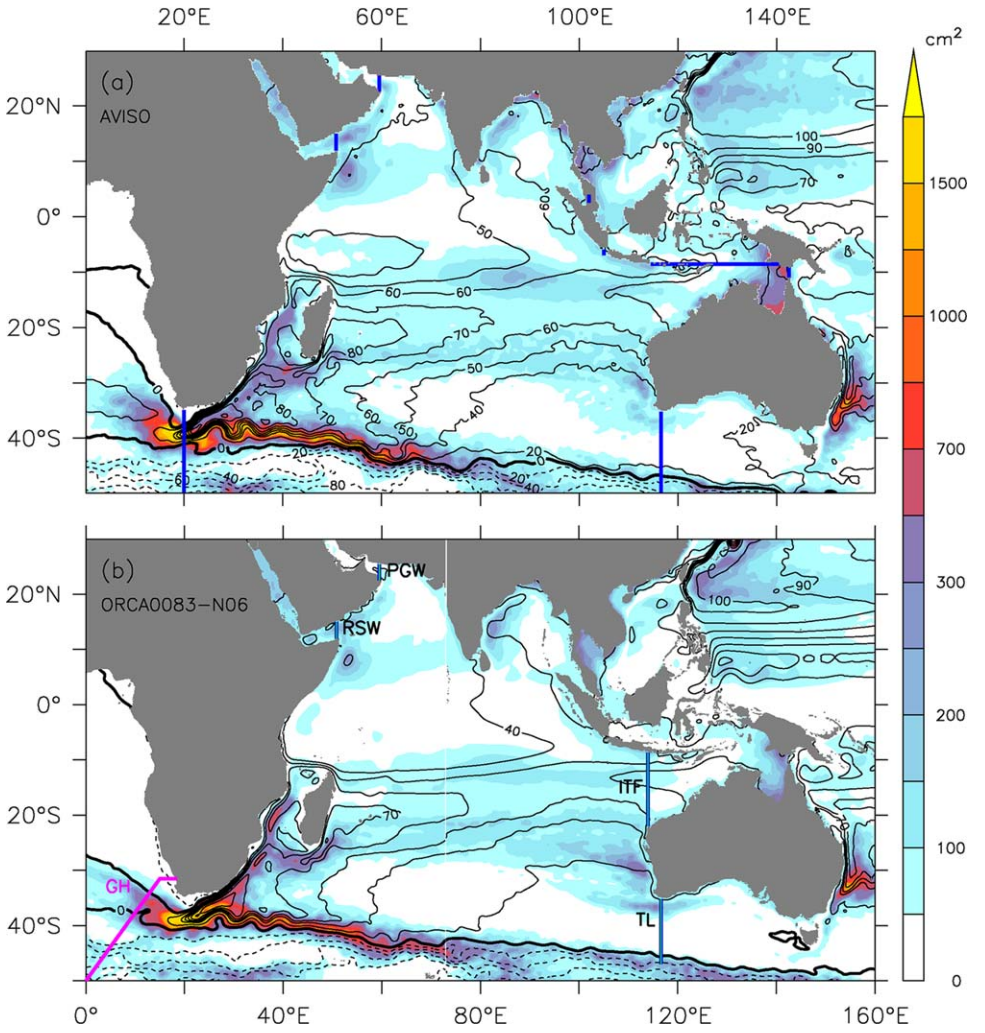

Figure 1. Representation of the mean circulation (contours of sea surface height, cm) and mesoscale variability (shading of sea surface height variance, cm^2) for the period 2000–2010 from (a) altimetric observations, AVISO, (b) model, ORCA0083. Sections in Figure 1a denote the final sections used for the quantitative Ariane experiments; sections at 20°E and 116.6°E extend to Antarctica. Sections in Figure 1b highlight the initial seeding sections used for the four main quantitative Ariane experiments. GoodHope (GH) is the section along which Agulhas leakage is commonly monitored.

The interconnectivity of the three southern hemisphere subtropical gyres allows for the secondary inflow of waters into the IO from the Pacific Ocean south of Australia, so-called Tasman leakage [*Ridgway and Dunn*, 2007; *Speich et al*., 2007]. Westward flow, in parts originating from the East Australian Current, is typically observed between Tasmania and the Subtropical Front [*Speich et al*., 2002]. Early observational and modeled estimates of this leakage give 0–13 Sv of thermocline and intermediate waters flowing westward south of Tasmania [*Rintoul and Sokolov*, 2001; *Speich et al*., 2002]. More recent studies constrain these estimates to around 4–5 Sv in the mean [*van Sebille et al*., 2012, 2014]. Derived from observational subsurface autonomous floats, *Rosell-Fieschi et al*. [2013] reported a westward transport of 5.2 ± 1.8 Sv at 115°E at intermediate depth. Despite the fact that both interocean exchanges north and south of Australia being of Pacific origin could arguably be related to large scale wind patterns [e.g., *Feng et al*., 2011], *van Sebille et al*. [2014] noted no obvious link between the two. Little is known on the spreading of Tasman leakage in the IO, but it is assumed to partly contribute to Agulhas leakage.

Other sources of surface and intermediate waters for the IO are from the marginal seas in the northwestern part of the basin (Figure 1). Resulting from extreme evaporation, warm, and saline water are formed in the Red Sea and Persian Gulf. These dense waters mix in the Gulfs of Aden and Oman due to high mesoscale activities [*Fratantoni et al*., 2006; *Al Saafani et al*., 2007; *L'Hégaret et al*., 2015]. In the Arabian Sea, they level

at depth between 200 and 900 m and spread equatorward [*Prasad et al*., 2001; *Bower et al*., 2002; *Chowdary et al*., 2005]. An analysis of historical hydrographic sections showed that the high salinities relative to the ambient waters could be traced within the Mozambique Channel and downstream in the Agulhas Current [*Beal et al*., 2000; *Roman and Lutjeharms*, 2007]. South of Africa, the high salinity waters undergo additional mixing and share the similar density classes as the relatively fresher but colder Antarctic Intermediate Water [*Beal et al*., 2006]. In the Cape Basin, *You et al*. [2003] reported about 0.4 $\pm$ 1 Sv of Red Sea Water entering the South Atlantic.

The outflow from the Indian Ocean into the Atlantic Ocean passes through a vigorous western boundary current regime southeast of Africa (Figure 1). The Agulhas Current transports warm and saline surface and intermediate water southward [*Lutjeharms*, 2006], with a typical transport of 84 $\pm$ 24 Sv (estimated from 3 years of mooring data) [*Beal and Elipot*, 2016]. The prominent contributors of water of the Agulhas Current are from the Mozambique Channel (16.7 $\pm$ 15.8 Sv, 6 years of mooring data) [*Ullgren et al*., 2012], from the South East Madagascar Current (37 $\pm$ 10 Sv, four hydrographic sections) [*Nauw et al*., 2008], and the rest from recirculations along the Agulhas Return Current [*Lutjeharms and Ansorge*, 2001; *Lutjeharms*, 2006]. The large standard deviations in transport value stem from the dominance of the mesoscale in this region (Figure 1). South of Africa, the Agulhas Current overshoots the shelf break and abruptly retroflects back into the Indian Ocean. The majority ($\sim$2/3–3/4) of the original Agulhas Current transport flows eastward as the Agulhas Return Current [*Lutjeharms*, 2006]. The remainder, roughly 15 Sv [*Richardson*, 2007], flows westward as Agulhas leakage mostly in form of mesoscale eddies, and constitutes the so-called warm and salty export into the South Atlantic that *Broeker* [1991] described.

Agulhas leakage in the Cape Basin can therefore in principle be decomposed into its various constituents: coming from the Pacific north and south of Australia, the marginal seas, and via the disparate sources of the Agulhas Current. The Cape Basin is, however, a cauldron, where waters of IO origin mix with ambient South Atlantic water and with waters from Drake Passage [*Stramma and England*, 1999], making it a challenge to identify and more importantly volumetrically quantify individual water masses from classical potential temperature-salinity plots.

The aim of this study is to decompose the exhaust of the IO, Agulhas leakage, into its individual sources using a high-resolution global ocean sea-ice model. We focus on waters of IO origin, determine and compare their pathways and associated timescales, and assess changes in properties along their way from the Pacific and marginal seas toward the Atlantic. The spreading of individual water masses in the IO has been described in the past using historical hydrography data sets, simple and coarse-resolution models [e.g., *You and Tomczak*, 1993; *You*, 1998; *Haines et al*., 1999; *Joseph and Swathi*, 1999; *Beal et al*., 2000; *Song et al*., 2004]. We use a Lagrangian analysis approach that allows us to follow entire water volumes (which may comprise of different water masses) and to provide quantitative measures by closing the IO inflow-outflow budget. For this study, we seek an understanding of the mean flow and do not resolve any variability on seasonal, interannual, decadal, or longer timescales. Nonetheless, it is important to note that the circulation of the IO is subject to changes on a range of timescales. For example, owing to the seasonality of the Asian monsoon winds, the upper ocean current system of the northern IO reverses biannually [*Schott and McCreary*, 2001]. On interannual timescales strong imprints of the Indian Ocean Dipole and the El Niño Southern Oscillation are observed [*Saji et al*., 1999; *Behera et al*., 2006; *Ummenhofer et al*., 2013]. As underlined by *Haines et al*. [1999], in order to adequately resolve the mean circulation, it is important that the Eulerian velocity fields used for the Lagrangian analysis incorporate the full temporal variability of the IO.

2. Methods

2.1. Model Output

The ORCA0083 configuration of the NEMO model (version 3.6) [*Madec*, 2016] is used for this study. This configuration, developed within the European DRAKKAR consortium [*The DRAKKAR Group*, 2007], simulates the ocean/sea-ice circulation nominally at 1/12° globally, which is eddy resolving between roughly 50°S and 50°N [*Hallberg*, 2013]. ORCA0083 uses an Arakawa-C staggered grid arrangement in the horizontal, and has 75 vertical levels, with 46 levels in the top 1000 m and spacing increasing from 1 m at the surface to a maximum of 204 m at depth. The experiment used for this study is the ORCA0083-N06, which was run by the National Oceanography Centre, Southampton, UK. The treatment of tracers is implemented using a

Laplacian operator for isoneutral horizontal diffusion (eddy diffusion of 125 m^2/s) and the total variance dissipation scheme for advection. Geopotential horizontal diffusion on momentum uses a bi-Laplacian operator (eddy viscosity of $-1.25e10$ m^4/s) and a vector form advection scheme conserving energy and enstrophy. Subgrid-scale vertical mixing is calculated through the turbulent eddy kinetic dependent diffusion scheme. This experiment started from rest with tracer fields initialized using a combined product derived from PHC2.1 [*Steele et al*., 2001], Medatlas [*Jourdan et al*., 1998], and *Levitus et al*. [1998], and was forced using the Drakkar Forcing Set (DFS5.2) [*Brodeau et al*., 2010; *Dussin et al*., 2014] for the period 1958–2012.

The first 5 years (1958–1962) of the simulation are treated as the initialization phase, so that for this study, 50 years output (1963–2012) are used. We note that a 5 years initialization phase is likely not sufficient to spin the whole overturning. However, it is sufficient for the circulation of the upper 1000 m in the IO (dynamic height fields difference between the first and last decades of the 50 years shows no major discrepancies, not shown). The three-dimensional velocity and tracer fields were stored at temporal resolution of 5 day means. *Qin et al*. [2014] showed that for offline Lagrangian analyses within models of similar horizontal resolution as ORCA0083, degradation in flow characteristics occurs when using model output with temporal resolution beyond 9 day average. The model's representation of the mean flow and of the variability of the IO region is adequate (Figures 1 and 2a). The region of high sea-surface-height variability in the source region of the Agulhas Current, which most nested configurations fail to reproduce adequately [*Biastoch et al*., 2008; *Durgadoo et al*., 2013], is well resolved by this simulation. Further details and overall evaluation of the model experiment can be found in *Moat et al*. [2016] and *Schulze* [2016].

2.2. Lagrangian Analysis of the Model Fields

Tracking water within the Eulerian output fields of the model was performed offline using the Ariane Lagrangian package [*Blanke and Raynaud*, 1997]. Ariane advects particles within the model fields by displacing them along analytically computed three-dimensional streamlines, taking advantage of the volume conservation property of the model, which implies that the velocity field has to be locally nondivergent. Unlike other explicit time-stepping methods, the analytical integration scheme yields unique and identical trajectory solutions both forward and backward in time.

Ariane runs in two complementary modes: quantitative and qualitative. In its quantitative mode, Ariane seeds particles along predefined sections at every time step (in this case, 5 day), whereby each particle is assigned a partial transport. The number of particles at each time-step is dependent on the transport across a particular section, such that the stronger the flow, the more particles are seeded; the cumulative transport of all particles represents the instantaneous Eulerian transport [*Blanke and Raynaud*, 1997]. Subsequently, the particles are advected forward or backward in time. Finally, they are captured when they cross edges of a predefined domain, and their transports are summed up. This mode is most useful to determine the connectivity between the seeding section and the edges of the predefined domain. A prime example where Ariane is successfully used in this mode is in measuring Agulhas leakage, defined by the portion of the Agulhas Current entering the Atlantic across the GoodHope line [*Durgadoo et al*., 2013; *Biastoch et al*., 2015].

Blanke et al. [1999] introduced the concept of the Lagrangian streamfunction based on the fact that Ariane respects mass conservation (nondivergent flow). As particles are advected in the quantitative mode their infinitesimal transports are summed at each velocity grid cell wall they cross. The resulting three-dimensional transport field can then be integrated vertically to obtain a two-dimensional locally nondivergent flow field that can be described by a horizontal streamfunction. Such a Lagrangian streamfunction thus represents the horizontal flow of the entire water volume that entered and left the study domain. Prerequisites are that first initial sections are seeded with sufficiently large number of particles, and second sufficient time is allowed for the particles to leave the domain across the defined final sections.

In the qualitative mode of Ariane, seeding positions are obtained by either first running a quantitative experiment or by user-defined start positions. Here, the former is favored since the particle positions derived from a quantitative experiment has the advantage of being tagged by partial transports. Furthermore, in qualitative mode, spatial and temporal information of individual particle trajectories are stored. Such information can subsequently be analyzed to assess pathways, timescales (e.g., *Rühs et al*. [2013] and

Lübbecke et al. [2015] for Agulhas water spreading in the Atlantic), and along-track changes in tracer properties.

Four main sets of Lagrangian experiments were performed for this study, each corresponding to the start positions of the particles at four different initial sections. These initial sections, illustrated in Figure 1b, capture water entering the IO basin from the Pacific Ocean (ITF and TL) and the marginal seas adjacent to the IO, namely from the Gulfs of Oman (PGW) and Aden (RSW).

1. PGW—meridional section at the mouth of the Gulf of Oman along 59.5°E; 22.5°N-25.4°N, where water enters the Arabian Sea.
2. RSW—meridional section at the mouth of the Gulf of Aden along 50.8°E; 11.9°N–15°N, where water enters the Arabian Sea.
3. ITF—meridional section along 114°E; between Australia (22°S) and Java (8.7°S). The Indonesian Throughflow is a collective term consisting of water transport across the Indonesian Archipelago through various Straits. Along 114°E, flow across 5 of the 7 Straits are captured, namely Lombok, Flores, Ombai, Timor, and Torres. Considering ITF collectively enables consistent analysis of pathways and timescales across the IO basin. Separate experiments for the two remaining Straits, Sunda, and Malacca, were performed, and shall be mentioned briefly in the results.
4. TL—meridional section along 116.6°E; between Antarctica and Australia (35.2°S). Strictly speaking, Tasman leakage occurs south of Tasmania [*Ridgway and Dunn*, 2007]. Here, since a sizable portion of the westward flowing water along this longitude between Australia and the Subtropical Front indeed originate from south of Tasmania [*van Sebille et al*., 2014], the nomenclature was deemed appropriate. The westward flowing Antarctic Coastal Current was not considered as part of TL, since it is confined south of the Antarctic Circumpolar Current and thereby does not enter the IO basin.

These four initial sections were designed to satisfy two criteria. First, the transport across each section is representative of the flow of the entire water column, including the respective water masses (as ordinarily measured along their typical isopycnals) after which they are named. Second, the sections are offset from the original water mass source, so as to minimize the effect of recirculations on timescales between the area where they originate and when they enter the IO.

The quantitative mode requires a closed domain to be defined, containing an initial section and several other final sections along which particles are captured. These final sections are shown in Figure 1a. The sections at 20°E and 116.6°E (TL) extend to the Antarctic continent. This domain was used for the quantitative experiments for PGW, RSW, and TL. For the ITF experiment, the final sections extending from Java to Papua (along 8.6°S) and New Guinea to Australia (along 142.5°E) were replaced with the initial section shown in Figure 1b.

So as to capture the interannual and decadal variability of the flow, it is necessary to seed particles over at least a few decades. In order to optimize the seeding strategy, and thereby allowing more particles to be seeded and integrated over a longer period of time, a series of preanalysis experiments was undertaken. In this preanalysis, particles were successively seeded full-depth along each initial section every 5 days over a period of 5 years, and were advected forward for a total of 25 years in quantitative mode. The initial positions of particles that, within 25 years, exited the domain south of Africa at 20°E were subsequently analyzed. It was found that over 99% of the particles reaching 20°E originated from PGW, RSW, ITF, and TL in the upper 500, 1500, 1500, and 1600 m, respectively (not shown). Furthermore, for the TL preanalysis experiment, the particles reaching 20°E originated from between Australia and 47°S, which roughly delineates the subtropical regime from the Antarctic Circumpolar Current (Figure 1). Repeating this preanalysis in reverse yields the same result (backward tracking of particles from 20°E to the four source regions). Results from the preanalysis experiments informed the design of the full set of Lagrangian experiments assessed here.

The four main sets of Lagrangian experiments were constructed as follows. Seeding across each initial section was refined based on the depth and latitude criteria described above. In quantitative mode, 1.5×10^6, 2.2×10^6, 10.1×10^6, and 10.0×10^6 particles were seeded every 5 days over a period of 30 years (1963–1992), corresponding to a total mean transport of 1.0, 3.6, 17.6, and 16.0 Sv across the PGW, RSW, ITF, and TL initial sections, respectively. The maximum accuracy achieved in this study is in the order of 0.1 Sv, therefore all transports reported here are rounded to 1 decimal place. The particles were then integrated forward for 100 years. Less than 3% of the initially seeded particles remained in the IO domain by the end of the

100 years. The long integration period was achieved by cycling twice through the input data, a practice previously employed for other studies of this kind [*van Sebille et al*., 2011; *Rühs et al*., 2013]. Out of 38.2 Sv (sum of the time-mean transport across the four initial sections), 23.2 Sv (60%, 3.8×10^6 particles) reached 20°E within 100 years, that is 0.3, 1.4, 10.9, and 10.6 Sv from PGW, RSW, ITF, and TL, respectively.

Subsequently, only those particles that exited the IO domain across 20°E were placed back at their respective initial seeding sections and advected forward in quantitative and qualitative modes for 100 years. The positions of the trajectories were stored every 5 days. Additionally, the modeled ambient temperature and salinity interpolated at the trajectory locations were stored at the same temporal frequency. Even though cycling through the input data allows for the analysis of longer pathways and timescales, the analysis of along-track tracer characteristics ought to be restricted to the length of input data available, that is, 50 years (see section 3.4).

3. Results and Discussion

3.1. Pathways from the Marginal Seas and the Pacific to the South Atlantic

We generated the Lagrangian streamfunctions after 100 years of integration, and in order to obtain a closed volumetric budget, particles remaining in the domain were omitted. Figure 2 shows the Lagrangian streamfunction for each experiment for all particles, while Figure 3 shows the same but for only those particles that exited the domain across 20°E within 100 years. In the first case, the isolines connect the initial seeding section with all other sections of the domain, and in the second case, they highlight only the flow from the seeding section to the section at 20°E south of Africa.

The 50 year mean Eulerian streamfunction, derived from annual average velocity fields, portrays the overall barotropic circulation of the IO basin (Figure 2a). Prominently, the two gyres of the south IO, roughly delineated along 10°S, are seen: the broad counter-clockwise south Indian subtropical gyre between 40°S and 10°S, and the narrow clockwise tropical gyre between 10°S and the Equator. Their associated western boundary currents, namely the Agulhas Current [*Lutjeharms*, 2006], the North and South East Madagascar Currents [*Swallow et al*., 1988], and the East African Coastal Current [*Swallow et al*., 1991], are also visible. North of the Equator, the circulation is strongly influenced by seasonal reversal of winds. A weak clockwise circulation illustrates a stronger summer (southwest) monsoon on average.

The total Lagrangian streamfunction (Figure 2b) portrays the vertically integrated flow of the four IO water sources. The resemblance to the Eulerian mean both in structure and magnitude suggests that it adequately captures the Eulerian circulation, hence validating the method. Generally, a congruity between the Eulerian and Lagrangian streamfunctions indicates that the prerequisites mentioned previously are sufficiently fulfilled. The biggest differences between the two fields probably stem from the fact that deep-water inflow (e.g., from the Atlantic across 20°E) is not considered and particle trajectories with potentially longer residence times in the IO (e.g., local recirculations in the Southwest IO) are prohibited to some degree by the experiment design (section 2.2). Also, it is worth noting that the Eulerian streamfunction portrays the circulation of the 50 year mean, while the Lagrangian streamfunction is based on trajectories with various residence times, up to 100 years [*Döös et al*., 2008]. The Lagrangian streamfunctions based on each individual experiments (Figures 2c–2f), showing the spreading of waters from the different source regions, are described next.

Water from the marginal seas entering the northwestern IO from the Gulfs of Oman and Aden show similar pathways (experiments PGW and RSW, Figures 2c and 2d). As they enter the Arabian Sea, these waters are advected equatorward and experience strong recirculation associated with seasonally varying flows [*Chowdary et al*., 2005; *Schott et al*., 2009]. Clearly distinguishable is the clockwise Great Whirl roughly centered at 9°N off Somalia, which recirculates both PGW and RSW waters predominantly during the southwest monsoon [*Beal and Donohue*, 2013]. At the mouth of the Gulf of Aden, RSW either veers immediately southward between the horn of Africa and the island of Socotra, or is advected westward into the Arabian Sea and into the interior of the northern IO. The former occurs during the northeast (winter) monsoon, while the latter during the southwest (summer) monsoon [*Fischer et al*., 1996; *Schott and Fischer*, 2000; *Prasad et al*., 2001]. *Beal et al*. [2000] analyzed historical hydrographic data, and reported a preferred spread of Red Sea Water along the African west coast through the Mozambique Channel. In contrast, the lack of direct contours in Figure 2d suggests the main RSW pathway consist first of an equatorial detour before reaching the

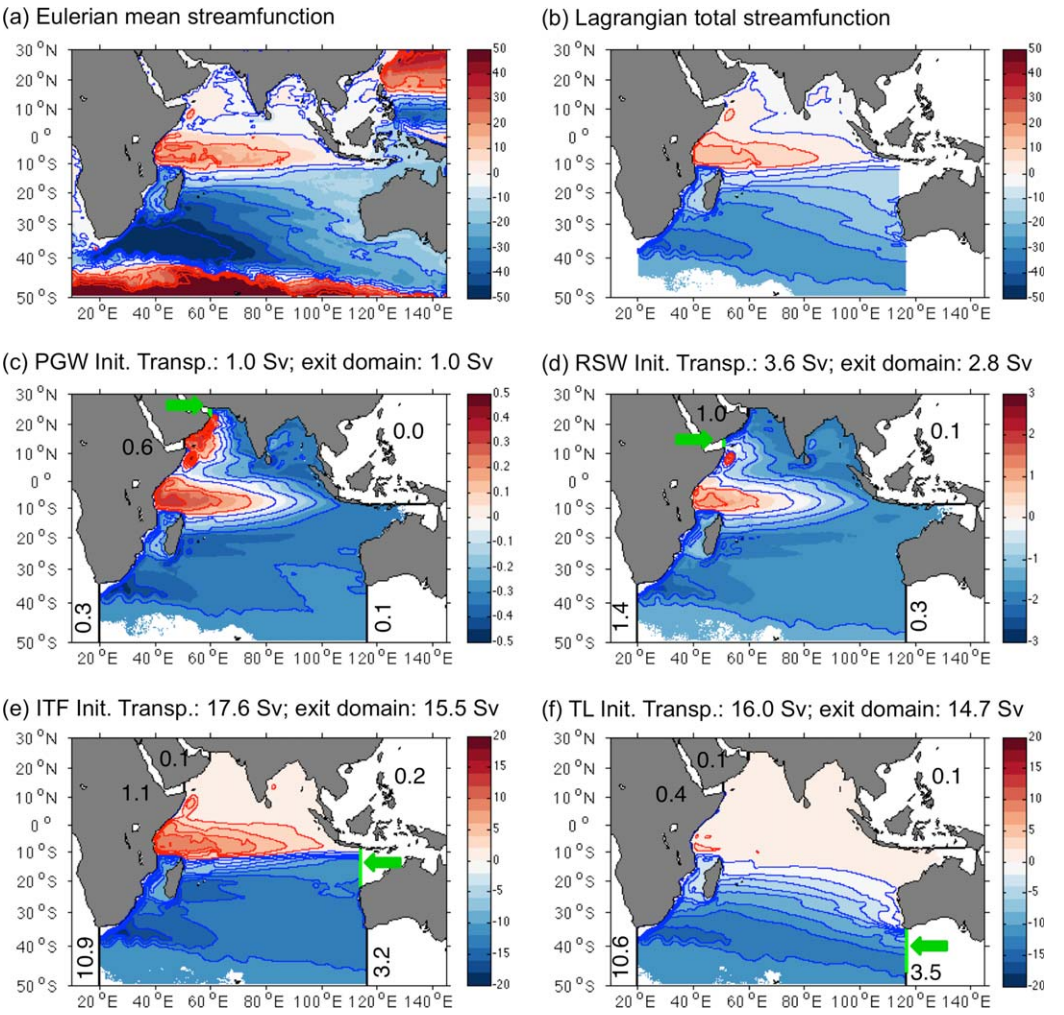

Figure 2. (a) Mean barotropic streamfunction from the Eulerian fields averaged over the period 1963–2012. (b–f) Lagrangian streamfunction derived only from particles that exited the domain within 100 years; reference set to 0 over Africa (20°E, Equator). (c–f) Streamlines showing the connection between the initial sections (PGW, RSW, ITF, and TL, highlighted by the green arrows) and the other final sections of the domain (black lines). Figure 2b is the sum of the four components shown in Figures 2c–2f. All units are in Sv.

Mozambique Channel. Dense water overflows are generally poorly resolved in z-level models and require special treatment [*Legg et al*., 2009]. ORCA0083-N06 contains no such special treatment for the overflows from the Gulfs; hence, Red Sea Water entering the Arabian Sea is lighter than expected. Being more surface bound in the model, waters from the Gulf of Aden is more prone to be affected by the seasonally changing circulation. And since the summer monsoon dominates the annual cycle, a preferred pathway into the Arabian Sea is likely. Furthermore, another difference between our study and that of *Beal et al*. [2000] is that we consider RSW as water exiting the Gulf of Aden over the full water column down to 1500 m, while *Beal et al*. [2000] focused on the spread of "pure" Red Sea Water along its typical density surfaces. Closed contours in the Bay of Bengal indicate some degree of spreading and residence there.

Along the Equator, water from both PGW and RSW broadly spread eastward, congruent with the South Equatorial Counter Current. Thereafter, between 10°S and 20°S, they flow back toward Madagascar within the South Equatorial Current and split. The bunching of streamlines north of Madagascar and through the Mozambique Channel highlights the preferred pathway toward the Agulhas Current. Averaged over the 30 years of seeding, 1.0 and 3.6 Sv, enter the Arabian Sea from the Gulfs of Oman and Aden, respectively. In the model about 0.17 and 0.15 Sv (Eulerian means over 50 years) exits the Persian Gulf at the Strait of Hormuz and the Red Sea at Bab al-Mandab Strait, respectively. These values fall within the reported observational range of 0.17–0.25 Sv for the Persian Gulf [e.g., *Bower et al*., 2000] and of 0.05–0.6 Sv for the Red Sea

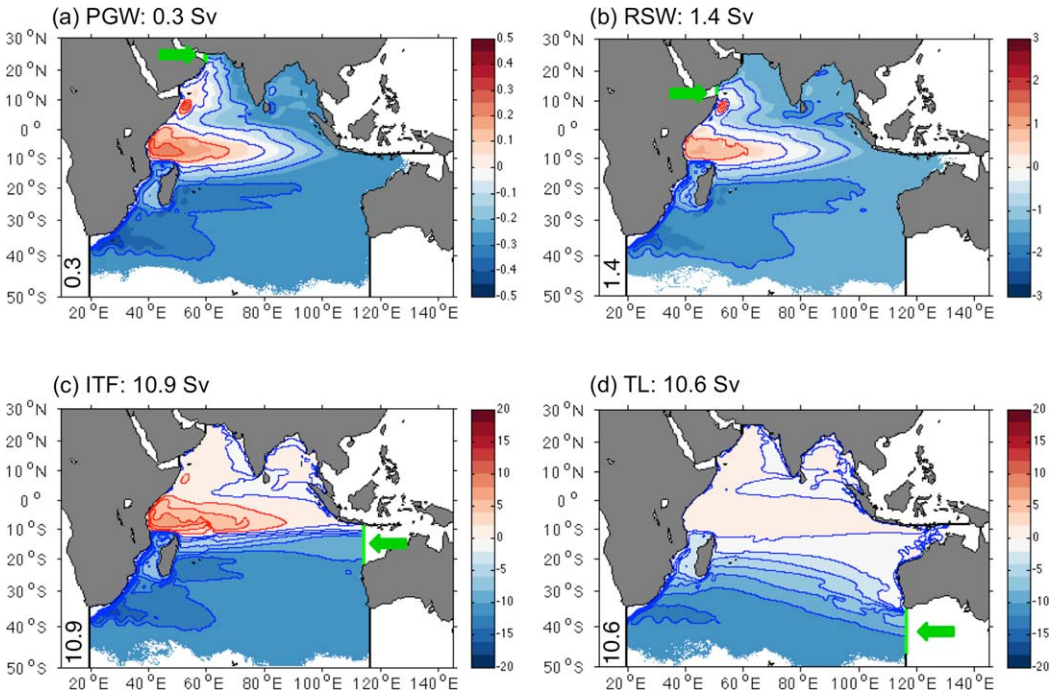

Figure 3. Similar to 2c–2f, but highlighting only the connectivity between initial sections (green arrows) and 20°E, that is no transport across the other final sections. 0.3, 1.4, 10.9, and 10.6 Sv from the initial sections PGW, RSW, ITF, and TL, respectively, reach 20°E within 100 years. All units are in Sv; Lagrangian streamfunction reference set to 0 over Africa (20°E, Equator).

[e.g., *Sofianos and Johns*, 2002]. Downstream of both Straits, mesoscale activities enhance the flow further. For example, *Fratantoni et al.* [2006] roughly estimated an additional 2–3 Sv flow through the Socotra Passage resulting from the propagation of Somali Current rings into the Gulf of Aden. Within 100 years, 0.3 and 1.4 Sv exit south of Africa from PGW and RSW, respectively.

Water entering the IO basin across 114°E from the Indonesian Archipelago is concentrated primarily in the top 600 m between the island of Java and 13°S. A shallower secondary core is centered at 21°S. Averaged over the 30 years of seeding, 17.6 Sv enters the basin in the top 1500 m (Figure 2e). This value falls within the observational range of 10.7–18.7 Sv [*Sprintall et al.*, 2009]. The major source of water at 114°E is through the Lombok, Ombai, and Timor Straits, with 3.3, 3.3, and 7.4 Sv, respectively (Eulerian means over 50 years); these values are also in agreement with *Sprintall et al.* [2009]. The bulk of the water is transported westward in a narrow band along 11°S till about 100°E, and is subsequently broadened feeding different branches of the South Equatorial Current. At the Mascarene plateau (59°E), two distinct branches of the South Equatorial Current are seen at 12°S and 16°S. The equatorward branch feeds the North East Madagascar Current, and bifurcates flowing through the Mozambique Channel and into the East African Coastal Current where it recirculates around the tropical gyre. Entry into the northern IO occurs along the African coast. The poleward branch feeds the South East Madagascar Current. In the southwest IO, streamlines from the Mozambique Channel and south of Madagascar converge in the Agulhas Current, and downstream either exit the domain or recirculate. Streamlines connecting the ITF section to the TL section indicate water exiting the IO basin south of Australia within 100 years either along the Agulhas Return Current and Subtropical Front (2.7 Sv), typically after first negotiating the retroflection south of Africa, or directly via the Leeuwin Current (0.5 Sv). About 60% (10.9 Sv) of ITF cross 20°E south of Africa within 100 years, with the most direct route being through the Mozambique Channel.

South of Australia (TL), 16.0 Sv entering the IO basin feed the broad westward flow of the south Indian subtropical gyre (Figure 2f). Most streamlines originating between Australia and 40°S spread either north or south of Madagascar, while those south of 40°S directly reach the Agulhas Current. Very little penetration of TL waters is observed in the northern IO, with only ∼3% being transported across the domain sections north of 10°S. This is likely due to the fact that TL waters are concentrated at intermediate depths (discussed

further in the subsequent sections), hence less prone to recirculate in the relatively shallow tropical gyre. More than 65% (10.6 Sv) of TL water exit south of Africa, and about 20% (3.5 Sv) recirculate leaving the domain again between 47°S and Antarctica.

Within 100 years, a total of 23.2 Sv from the four source regions reach south of Africa at 20°E. Figure 3 highlights only the pathways connecting each individual component to the section at 20°E. Since by design (preanalyses in section 2.2), water entering the IO basin are predisposed to leave the domain at 20°E if allowed sufficient time, the overall pathway depicted in this subset is similar to that shown in Figures 2c–2f. Most notable differences are: (1) Detours north of the Equator are less prominent in the cases of ITF and TL. (2) Recirculation of TL in the southwest IO is much weaker. This indicates that the pathway between TL and 20°E is for the most part direct and via the South East Madagascar Current.

Figure 4 schematically summarizes the most likely pathways shown in Figure 3 from the four source sections toward 20°E and subsequently into the Atlantic. Additionally, the origins of the contributions from ITF and TL are further decomposed. The partitioning of ITF waters coming across Lombok, Ombai, and Timor Straits and reaching 20°E within 100 years reflects that of the total transport across the ITF initial section, namely roughly 60% (cf. Figure 2e and the Eulerian means for the transport across the Straits given above). For TL, a large portion of the 10.6 Sv comes from recirculations across the initial section [*Sallée et al*., 2006]. The portion originating from between Tasmania and 50°S as Tasman leakage (3.1 Sv) commensurate previous findings [*van Sebille et al*., 2012, 2014; *Rosell-Fieschi et al*., 2013].

Of the 23.2 Sv that flows across 20°E within 100 years, 90% flows either through the Mozambique Channel or southeast of Madagascar. Waters from PGW, RSW, and ITF flow preferably along the South Equatorial Current and through the Mozambique Channel, while TL waters predominantly either are incorporated within the South East Madagascar Current or flow directly westward. After crossing 20°E, a little more than 50% of the waters proceed to leave the IO basin across GoodHope, the rest retroflects. Of the 12.2 Sv entering the Atlantic, over 96% were previously within the Agulhas Current, and can therefore be referred to as part of Agulhas leakage (as opposed to the more general term "Indian Ocean leakage").

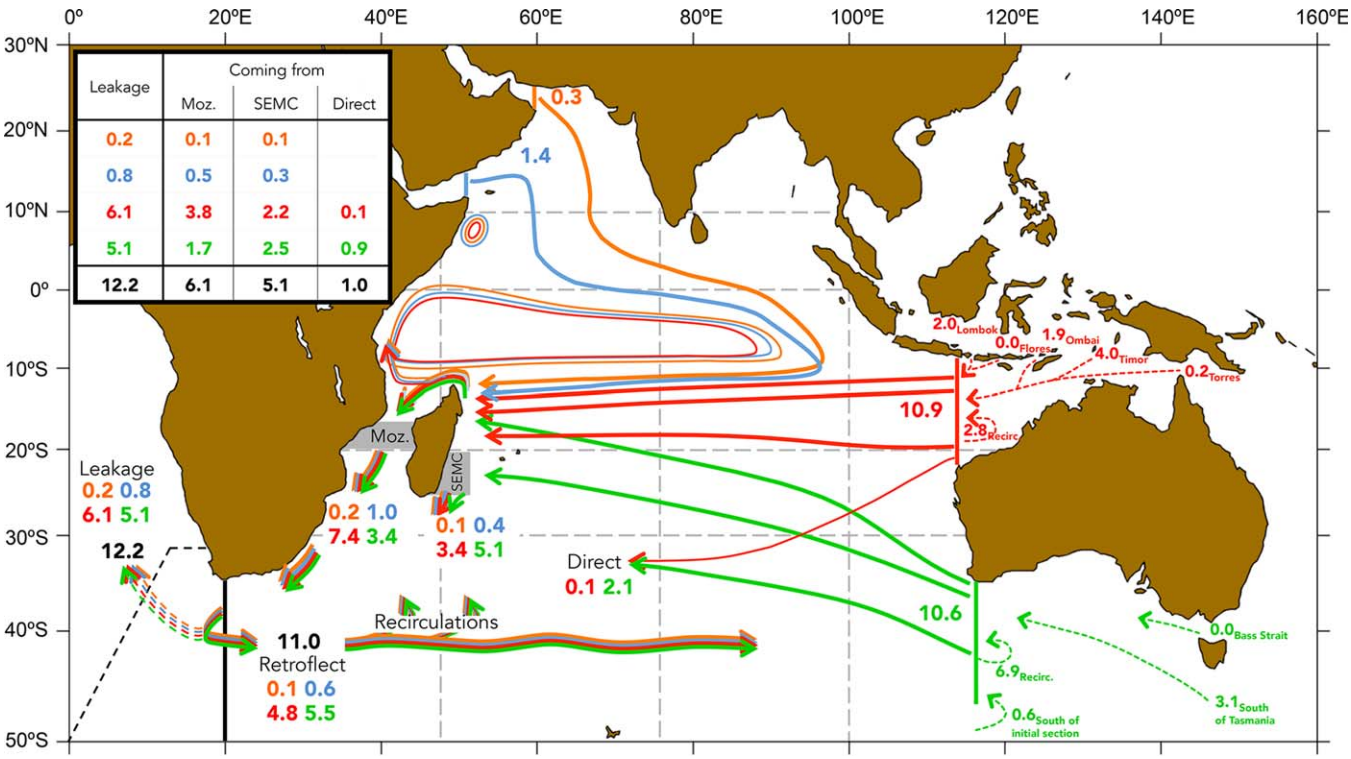

Figure 4. Schematic of the major pathways of water crossing 20°E within 100 years from the Indian Ocean. Of the 23.2 Sv from the four source regions, PGW (orange), RSW (blue), ITF (red), and TL (green), 12.2 Sv enters the Atlantic across the GoodHope section (dashed black line), the rest retroflects (11.0 Sv). Agulhas leakage within the model is 14.1 ± 2.2 Sv (see text for details). Sizes of arrows vary for clarity purposes. The table details the decomposition of leakage. Dashed arrows itemize the upstream sources of ITF and TL. Transport numbers are in Sv.

The ratio of water last seen leaving the grey shaded boxes (Figure 4) in the Mozambique Channel (Moz), southeast of Madagascar (SEMC), and arriving directly at 20°E without going through the Channel or southeast Madagascar are 5:4:1 (total of 23.2 Sv). There are no direct routes from the marginal seas to 20°E within 100 years, and water from the Gulfs of Oman and Aden flows either through the Mozambique Channel or through the Southeast Madagascar Current. Moreover, comparing the volume transports of particles' first entry into the grey shaded boxes and those last seen leaving them, there is a 20–25% chance that water entering the Channel or the South East Madagascar Current will recirculate within the southwest IO gyre, re-enter the Channel or the Southeast Madagascar Current, before eventually exiting at 20°E (also seen in Figure 3). The exception is for water from TL arriving southeast of Madagascar, where recirculation is negligible (weaker recirculation in the southwest IO in Figure 3d).

Agulhas leakage is commonly defined as the portion of the Agulhas Current, for example, at 32°S that leaks into the Atlantic across the GoodHope section within 3–5 years, and is intuitive measured in models using a Lagrangian framework [*Durgadoo et al*., 2013; *Biastoch et al*., 2015; *Lübbecke et al*., 2015]. In the present model, employing this definition and over the period 1963–2008, the mean value of Agulhas leakage is 14.1 Sv with an annual standard deviation of 2.2 Sv. This value falls well within the expected range [*Richardson*, 2007]. In the schematic (Figure 4), we show that Agulhas leakage can be decomposed on average as ∼1 Sv arriving from the marginal seas of the northwest IO and ∼11 from the Pacific through the Indonesian Archipelago (∼6 Sv) and south of Australia (∼5 Sv), totalling ∼12 Sv. The missing ∼2 Sv could stem first from the so-called cold-water-route at intermediate depths from the south Atlantic [*Rimaud et al*., 2012; *Rusciano et al*., 2012] and second from the two remaining Straits not covered by the ITF section, namely Sunda and Malacca. As mentioned in section 2.2, separate Lagrangian experiments were additionally performed for the two Straits. They contribute ∼0.4 Sv to Agulhas leakage. To estimate the portion of South Atlantic origin, a backward experiment was performed where particles were seeded along the GoodHope section between Africa and 50°S in the top 2000 m for 30 years and advected backward in time for a total of 80 years to determine their origins. Of the ∼14 Sv of Agulhas leakage seeded, ∼0.9 Sv originated poleward of 50°S across 0°E from the South Atlantic, ∼0.8 Sv originated from below the GoodHope section deeper than 2000 m. Thereby, all the constituents of Agulhas leakage are accounted for.

Typically, 20–25% of Agulhas Current water leaks into the Atlantic. The Eulerian mean Agulhas Current transport at 32°S (Figure 2a) in the model is ∼63 Sv (falls within observational uncertain range of *Beal and Elipot* [2016]), of which ∼14 Sv leaks (classical definition), meeting the expectation. From the total Lagrangian streamfunction (Figure 2b) the Agulhas Current at 32°S is 33 Sv (of which, PGW: 0.4 Sv, RSW: 2.2 Sv, ITF 16.4 Sv, TL: 14 Sv; Figures 2c–2f), meaning that the current draws about half of its water from the four source regions considered here. The remainder is drawn from water recirculating along the Agulhas Return Current and Subtropical Front [*Lutjeharms and Ansorge*, 2001; *Lutjeharms*, 2006].

3.2. Timescale Across the IO and Into the South Atlantic

The timescales associated with the flow from the source regions toward GoodHope are shown in Figure 5. Each box plot shows the temporal distribution in transport first crossing the respective latitudes and longitudes of only those particles that cross the GoodHope section as Agulhas leakage (12.2 Sv in total).

The westward transport of water from ITF and TL is mainly achieved by the mean flow with the core of the ITF waters being in the top 500 m and TL below that. Within the IO subtropical gyre between 60°E and 100°E the fastest modeled mean speeds are ∼0.1 m s^{-1} in the top 500 m and ∼0.02 m s^{-1} between 500 and 1000 m (not shown). Therefore, between the ITF and TL initial sections and 77°E, approximately 4200 km apart, a particle traveling at these speeds, would take ∼1.3 years in the top 500 m and ∼6.7 years below that. These values are consistent with the fastest timescales shown at 77°E, indicated by the lower edges of the boxes in Figure 5b, where 25% of the transports reach the section in less than 1.2 and 6.4 years, respectively. This and the narrow interquartile ranges of the boxes, suggest that only minor stirring occurs until 77°E.

Waters from PGW being more surface-bound than those from RSW are likely to recirculate and linger in the northern IO. The bulk of the RSW waters (75% of it) cross the Equator twice as fast as PGW waters. Detours in the Bay of Bengal further account for the long timescales in the northern IO. The slowest particles are delayed by more than 2 decades between the Equator and 20°S due to residence within the tropical gyre.

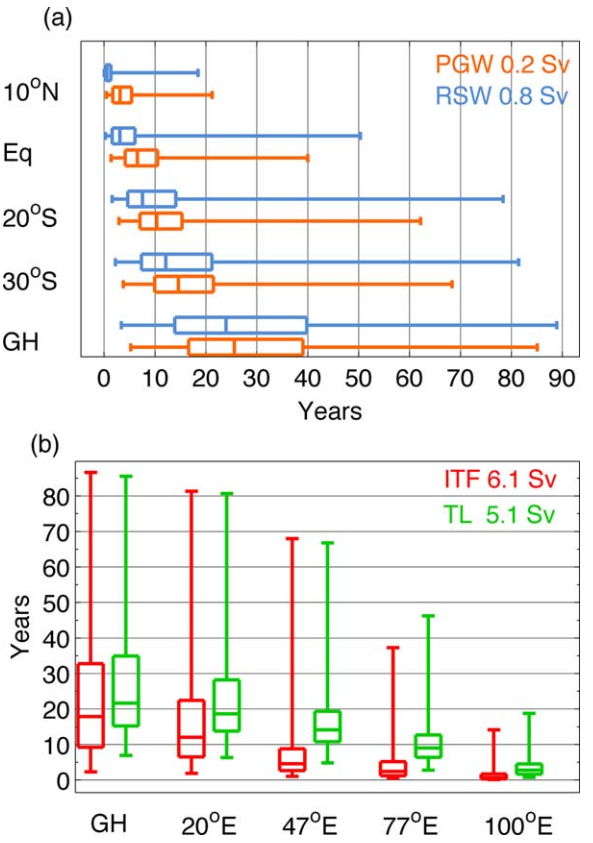

Figure 5. Transit time within the Indian Ocean of water eventually entering the Atlantic within 100 years from PGW (0.2 Sv, orange), RSW (0.8 Sv, blue), ITF (6.1 Sv, red), and TL (5.1 Sv, green). Each box plot shows the temporal spread in transport reaching the respective lines of longitudes and latitudes (grey dash lines in Figure 4). The edges of the boxes delineate the 25 and 75 percentiles, and the medians are indicated as lines across the boxes. The tails encompass 99% of the transport from the respective sources reaching GoodHope (GH) as part of Agulhas leakage.

In the southwest IO south of 20°S between 20°E and 47°E, the elongated boxes and extended tails indicate that the recirculatory and highly eddying nature of the flow there affect timescales of water from all origins (cf. Figure 1).

At GoodHope, the fastest waters are from ITF, with 25% of the volume transport arriving within the first decade. The relatively direct pathways of water of Pacific origin in contrast to those from the marginal seas are evident from the length of the respective lower tails in Figure 5. About half of the water transported into the Atlantic from all sources occurs within 25 years. Worth noting is that within 50 years, which is the length of one cycle of model data used, over 75% of the transport across GoodHope are accounted for.

3.3. Depth Structure of Waters Entering the South Atlantic

Within the Lagrangian framework, it is possible to examine the depth characteristics of waters of disparate sources along the GoodHope section as they enter the South Atlantic and before. The depth distribution of particles that cross GoodHope as Agulhas leakage and were last seen leaving the Mozambique Channel (across 20°S) or the Southeast Madagascar Current (across 25°S, 47–52°E) are shown in Figure 6. The mean flow is in both cases intensified along the coast to the left (cf. Figure 1), in the Mozambique Channel in the upper 500 m and southeast of Madagascar below that. The dominance of waters of ITF origin in the Mozambique Channel (3.8 out of 6.1 Sv) and of waters of TL origin southeast of Madagascar (2.5 out of 5.1 Sv) is evident and in line with the results described in section 3.2 for the entire transport reaching 20°E within 100 years. Southeast of Madagascar, there is additionally a clear delineation in the vertical between the waters of Pacific origin above and below 500 m. Red Sea Water, as a water mass, is typically found in the southwest IO at intermediate depths [*You*, 1998; *Beal et al*., 2000; *You et al*., 2003]. Here, in the upper layer above 750 m, waters of RSW origin can be found on either side of Madagascar. At intermediate depth, however, a sizable amount of RSW water can only be detected in the Channel corroborating previous reports [e.g., *You*, 1998; *Beal et al*., 2000). The contribution of PGW is small and confined to the surface. Within the Agulhas Current, unlike the quasi-instantaneous observations of *Beal et al*. [2006], who found distinct water of distinct origins on either side of the current's core, here, no such clear demarcation is noted (not shown).

Agulhas leakage waters cross GoodHope mostly between 8°E and 18°E in the top 1250 m (Figure 6a), consistent with the broad fan of enhanced sea surface height variability in Figure 1b. In contrast to the relatively clear depth separation of ITF waters overlying TL waters within the subtropical gyre and southeast of Madagascar, at GoodHope (similar to within the Agulhas Current further upstream), these two water sources are mixed throughout the water column. Nonetheless, integrated across the section, ~4.5 Sv of ITF waters are concentrated in the top 500 m, while the same amount of TL waters are mostly centered between 250 and 1000 m. *van Sebille et al*. [2010] previously examined the question of what determines the fate of Agulhas water crossing 20°E. At that longitude, they noted a fairly similar spread in waters leaking into the

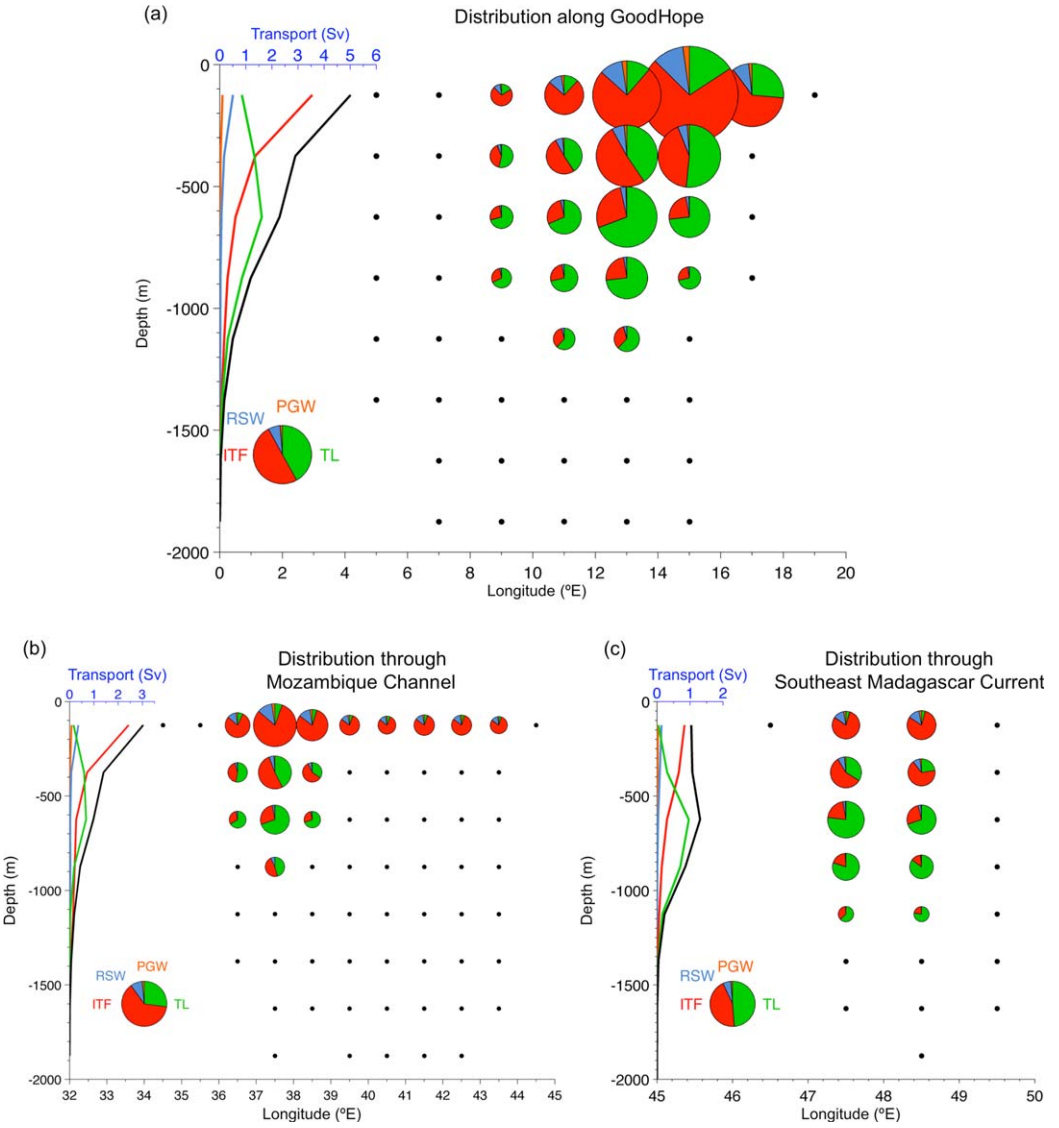

Figure 6. Transport depth-longitude distribution of waters from four origins that exit the Indian Ocean within 100 years across the (a) GoodHope section, and having passed through the (b) Mozambique Channel or (c) Southeast Madagascar Current immediately prior exiting (grey shaded boxes in Figure 4). Color coding given in legend. Each pie chart represents the transport through 1° or 2° of longitude × 250 m, with 1 Sv scaled to represent size of the pie chart in the legend. Pie charts with total transports less than 0.1 Sv are indicated by dots instead. The left plots show the zonally integrated transport as a function of depth, with the black curve showing the sum of the four components. Partitioning shown in the legend correspond to the total depth-integrated transport of (a) 12.2 Sv (0.2, 0.8, 6.1, and 5.1 Sv for PGW, RSW, ITF, and TL respectively); (b) 6.1 Sv (0.1, 0.5, 3.8, and 1.7 Sv for PGW, RSW, ITF, and TL respectively); and (c) 5.1 Sv (0.1, 0.3, 2.2, and 2.5 Sv for PGW, RSW, ITF, and TL respectively).

Atlantic and to those returning to the IO. This lent support to the mechanism of ring shedding by loop occlusion [*Ou and de Ruijter*, 1986] as the dominant factor in determining the fate of water crossing 20°E. With the exception of TL, values shown in Figure 4 suggest more water of PGW, RSW, and ITF origins to enter the Atlantic than to retroflect. It is important here to keep in mind the transport still left in the domain after 100 years of integration, which provides an upper bound of the uncertainties in this discussion (headers in Figures 2c–2f). A detailed look at the overall depth distribution at 20°E of waters leaking in contrast to those retroflecting shows a general agreement with the conclusion of *van Sebille et al*. [2010]. This distribution is unchanged from that upstream within the Agulhas Current. In the upper 250 m all sources but TL exhibit a preference for leaking. This is likely because of the surface-intensified cyclonic relative vorticity [*van Sebille et al*., 2010]. Below 500 m, waters of TL origin have a slight tendency to more likely retroflect than leak.

3.4. Water Properties Modification Within the Indian Ocean

From a Lagrangian connectivity perspective, we have investigated thus far the advective pathways and timescales of water from the source regions to the Atlantic. The question remains: to what extent does the Indian Ocean modify the water mass characteristics of the inflowing waters before exporting them? Here we consider the memory of the bulk water volume as opposed to that of individual particles or water masses.

Every 5 days, potential temperature (θ) and salinity (S) were linearly interpolated from the tracer fields onto each particle location. Inherently the tracer field incorporate the simulated and parameterized turbulent motions of the model, including the air-sea fluxes (described in section 2.1). For the purpose of examining the modification of water characteristics within the IO, only the first 50 years of the trajectories were considered. We noted from Figure 5 that more than 75% of water from the Pacific and the marginal seas reaches the Atlantic within 50 years. Figure 7 shows normalized transports binned according to potential temperature θ, salinity S, potential density anomaly σ_0, and depth of particles at their origins, at the first time they cross meridional and zonal sections across the IO, and finally as they exit across GoodHope within 50 years (sections shown in Figure 4). In the upper plot of Figure 7, the two distributions for "Init" are equivalent.

Waters from the marginal seas of the IO are typically characterized by their high salinities [*Beal et al*., 2000; *Bower et al*., 2000; *Chowdary et al*., 2005]. Initially waters from the Gulfs of Oman and Aden have distinct characteristics ($\theta > 20$°C; S > 35.5), as evidenced by the shapes of the respective distributions (Figures 7a and 7b) being narrow and single peaked. Since only first crossing is considered, the broadening of the respective salinity distributions along 10°N indicates that these waters rapidly mix with ambient waters of the Arabian Sea. From this point, they become indistinguishable. Between 10°N and the Equator, while the potential temperature distributions of PGW and RSW waters remain alike, a salient freshening is noted. Furthermore, the initial θ–S signatures of the waters are lost. The densest RSW waters at intermediate depths ($\sigma_0 > 25$ kg/m^3) however maintain some of their relatively high salinity signatures. During the transit within the southern IO, the salinities remain relatively similar, but a gradual cooling occurs. Waters that do not directly exit at GH, and instead first recirculate within the south IO subtropical gyre undergo further erosion in properties.

Pacific waters through the Indonesian Archipelago are characterized by their relatively lower salinities (S < 35.5) and broad potential temperature distribution. The direct and fast (cf. Figure 5) westward advection within the South Equatorial Current results in little change in water properties. Upon reaching Madagascar along 47°E and further west, shifts in distributions are noted indicating mixing (Figure 7c).

Waters entering the IO south of Australia are predominantly confined at intermediate depths between 500 and 1000 m, and undergo only slight changes in properties as they transit westward across the basin. The reduction in amplitude and slight broadening of the distributions (Figure 7d) indicate minor erosion of properties and mixing with surrounding water masses below and above.

Within the model, waters from the Gulf of Oman lose their initial characteristics rapidly within the Arabian Sea. South of the Equator, their high salinity signature is no longer detectable. This is similar to surface waters from the Gulf of Aden. At intermediate depths, a very small amount of high salinity waters from the Red Sea persists into the southern IO (model deficit discussed in section 3.1). In contrast to the rapid decay of waters from the marginal seas, waters from the Pacific north and south of Australia maintain their properties for most of their westward crossing. At GoodHope, the properties of waters originating from the Gulfs and from the ITF are almost indistinguishable (Figures 7a–7c), consistent with the volumetric depth distribution (Figure 6a). In contrast, the properties of waters from south of Australia cross GoodHope almost intact.

In general, water modification is possible by either mixing with ambient waters or via surface fluxes. We first consider the former. Salinity fields in the IO along the isopycnals at which water from the four source regions enter the basin show that the largest gradients occur in the northern IO (Figure 8). Waters from the Gulfs enter a region of sharp contrast in the Arabian Sea favoring immediate isopycnal mixing. ITF enters the IO basin over a relatively broad range of densities in the upper 500 m. At its surface and subsurface-intensified core (σ_0 22–23 kg/m^3), it enters the basin in regions of weaker salinity gradients. Along isopycnal mixing starts to occur at about 80°E and is gradual until Madagascar (47°E). Weak gradients in the southern IO, in addition to little to no contact with the surface and weak recirculations in the southwest IO, result in water from TL transiting the basin experiencing only minor erosion.

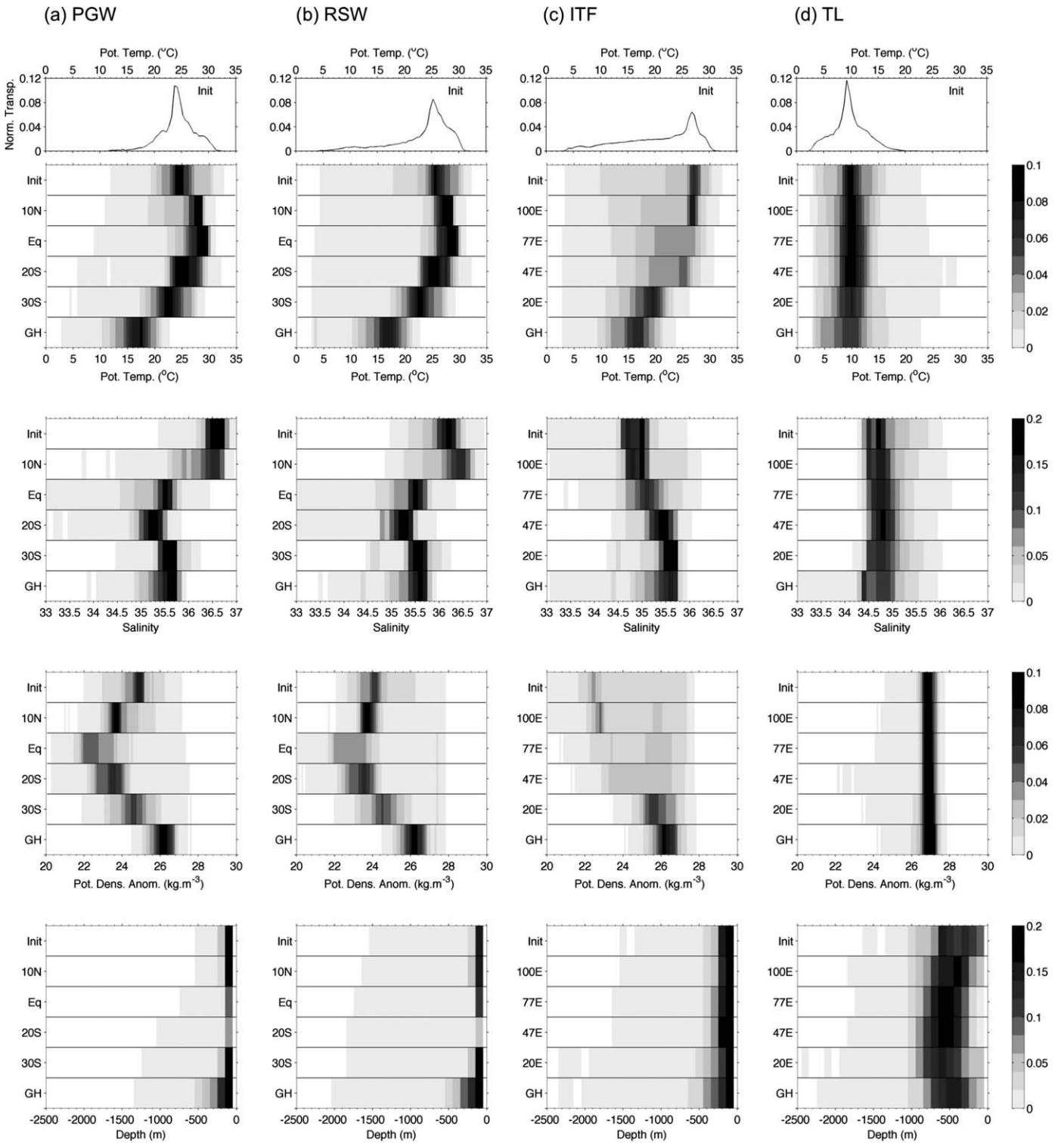

Figure 7. Normalized transports (units Sv/Sv) binned by potential temperature (upper plot, °C), salinity (middle-upper plot), potential density anomaly (σ_0, middle-lower plot, kg/m^3), and depth (lower plot, m) at the initial positions (Init), at the first crossing of 4 meridional/zonal sections across the Indian Ocean basin (sections shown in Figure 4), and at GoodHope (GH). In the upper plot, the potential temperature "Init" histogram and the "Init" strip are equivalent, in that the horizontal strip is a top view of the histogram. The transport distributions were normalized by the total transport of each component: (a) 0.1 Sv, (b) 0.5 Sv, (c) 4.6 Sv, and (d) 3.7 Sv entering the Atlantic within 50 years from PGW, RSW, ITF, and TL, respectively. The bin intervals are 0.5°C, 0.1, 0.1 kg/m^3, and 100 m, respectively.

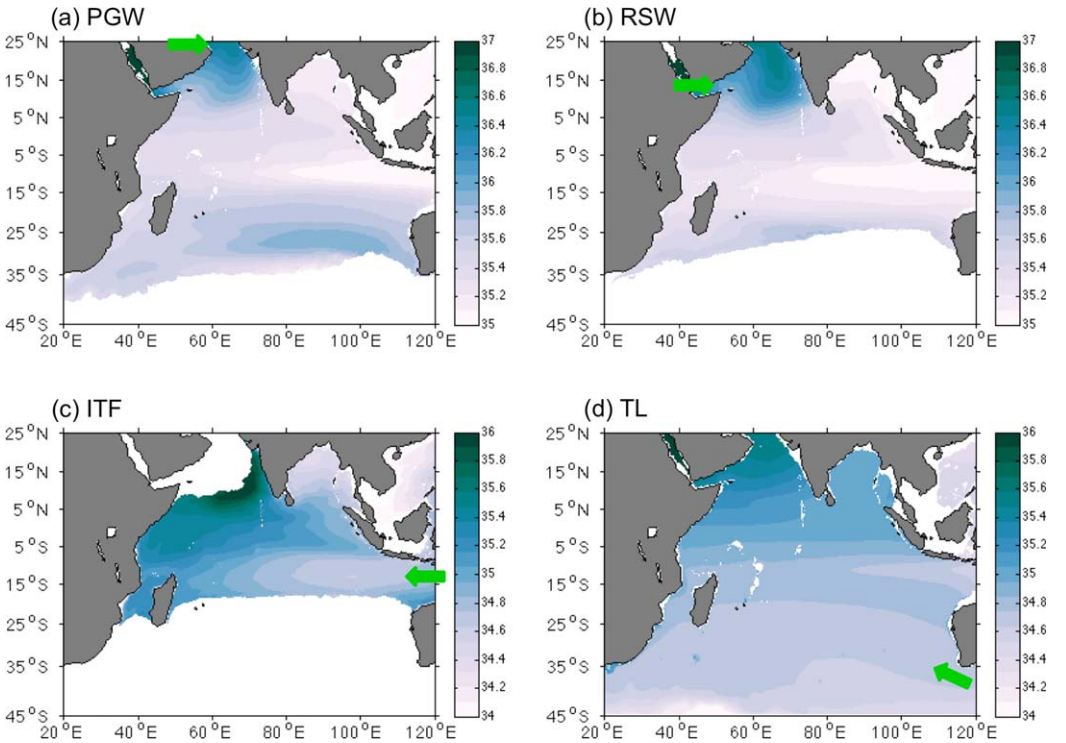

Figure 8. Salinity from the Eulerian fields averaged over density classes representative of the bulk of water entering the Indian Ocean basin (initial sections, green arrows) for the period 1963–1992 from PGW (σ_0 = 24.5–25.5 kg/m^3), RSW (σ_0 = 23.5–24.5 kg/m^3), ITF (σ_0 = 22.0–23.0 kg/m^3), and TL (σ_0 = 26.5–27.5 kg/m^3).

Biastoch et al. [2015] calculated the heat transport across GoodHope within a model with different atmospheric forcing by integrating full-depth from Africa to the dynamic boundary delineated by the Subtropical Front. Applying the same method, we obtain 0.35 ± 0.04 PW (1963–2012, using annual-mean values), which roughly agrees with their estimate. Does the heat exported across GoodHope come from the Pacific, or mostly set by surface fluxes within the IO basin? Waters from the Gulfs and ITF lie predominantly in the upper 250 m (lower plot Figure 7) and therefore experience modifications resulting from surface fluxes. Within the model and in agreement with observations (not shown), the net surface heat flux exhibits a flux into the ocean in the northern IO, and flux to the atmosphere within the subtropical gyre and the greater Agulhas Current system. Since volume is conserved for all particles, integrating under the curves of Figure 7 (upper plot) yields normalized transport weighed potential temperature (TWT) values for the bulk of the water from the four origins. At the source (init), the waters entering the IO have a TWT of 16°C (PGW = 24°C, RSW = 23°C, ITF = 21°C, TL = 10°C). Overall, at GoodHope, the waters are 3°C cooler (PGW = 16°C, RSW = 15°C, ITF = 15°C, TL = 9°C), suggesting that the IO cools the waters it receives. Figure 7 shows that this cooling occurs over the greater Agulhas Current system, consistent with the model's net heat flux to the atmosphere. In the Arabian Sea, north of the Equator, the temperature distributions of PGW and RSW indicate heat gain, which is also consistent with the sign of the net heat flux there. This therefore suggests that exchange with the atmosphere over the IO basin is an important factor determining the heat exported to the South Atlantic.

The fresh water export of the IO is −192 ± 34 mSv (also calculated following *Biastoch et al.* [2015] and agree with their value), and for the most part, waters from the ITF salinificate, while those from the Gulfs freshen.

4. Summary and Conclusions

We investigated the mean pathways, transit timescales, and transformation of waters flowing from the Pacific Ocean and the marginal seas through the Indian Ocean (IO) on their way toward the South Atlantic. Lagrangian analyses of Eulerian fields from a high-resolution ocean/sea-ice model were performed. Particles were released over a period of 30 model years along sections that define the entry points of water into the IO basin: at the mouths of the Gulfs of (1) Oman and (2) Aden, (3) north and (4) south of Australia. The

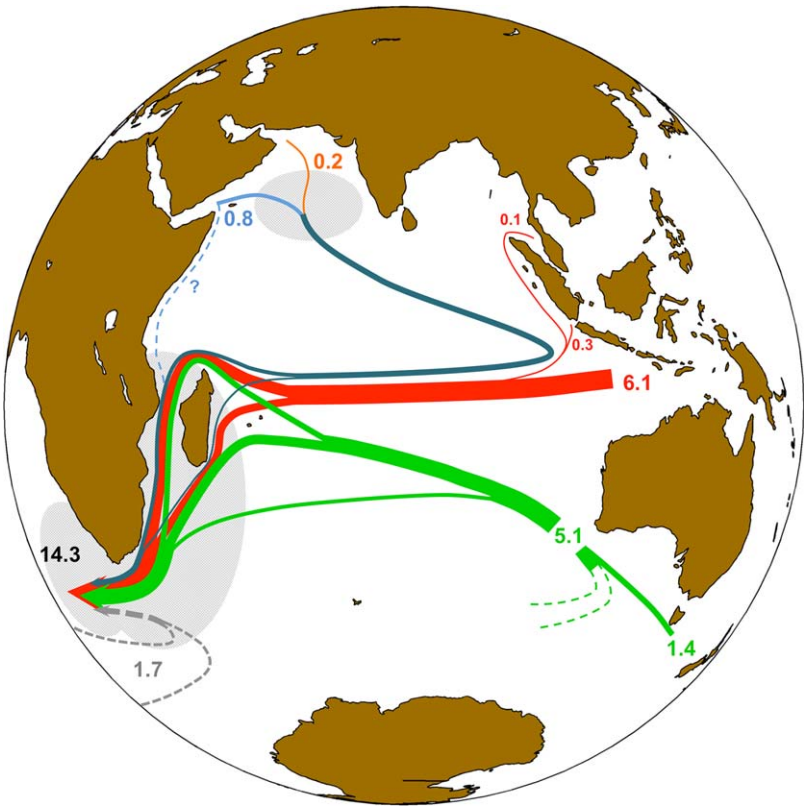

Figure 9. Schematic decomposition of sources of Agulhas leakage and their mean pathways within the Indian Ocean. Line/arrow thickness represents the different transport (Sv) contribution (see table in Figure 4). Indonesian Through-flow (red) additionally receives water from Sunda and Malacca Straits. Waters from south of Australia (green) consist of Tasman leakage and recirculations. Waters from the Gulfs (blue and orange), leaving the Arabian Sea share similar properties (represented thereafter in teal). A possible route from the Gulf of Aden along western Africa is shown but not quantified (dashed blue, see text for details). Finally, Agulhas leakage also receives water from the Atlantic (dashed grey arrow). Grey shaded areas denote region where strongest changes in water properties occur.

experiments were design so as to decompose and quantify the constituents of the exhaust of the IO, namely Agulhas leakage, and to determine whether the IO acts as a passive connector or plays an active role as a modifier.

Agulhas leakage (AL) in the model is roughly 14 Sv, which is within the observed range (section 3.1). Based on results from this study, Figure 9 shows the volumetric decomposition and the pathways of the sources of AL. The principal contributor of AL comes from north of Australia as Indonesian Through-Flow (ITF, 45%, 6.5 Sv). More than half of that water flows through the Mozambique Channel within 5 years, where it is mostly confined in the upper 500 m along the African coast. Waters from Sunda and Malacca Straits were not explicitly discussed here. They contribute around 0.4 Sv to AL. The second contributor of AL, 5.1 Sv, originates from south of Australia, of which 30% (1.4 Sv) come directly from the Pacific as Tasman leakage, and the rest from recirculations from the frontal regions of the Southern Ocean. Within the IO, these waters sit at intermediate depths and slowly transit westward within the subtropical gyre, reaching the Agulhas Current in about 2 decades mostly via the Southeast Madagascar Current (50%). About 20% flows directly into the Agulhas Current. In the model waters from the Gulfs contributing to AL (1.0 Sv) have similar pathways, which first consist of a detour toward the northeastern IO before subsequently converging within the boundary currents on either side of Madagascar. Deficits in the model result in a negative density bias (lighter than observed) for waters entering the IO from the Gulf of Aden. Therefore, their pathways north of 10°S portrayed in Figure 9 may be overly influence by the seasonally reversing upper ocean circulation there. Consequently, while our results do not suggest a direct route from the Gulf of Aden along western Africa (blue dashed line in Figure 9) as reported by *Beal et al.* [2000], we cannot discount it as a possible route. Finally, also not explicitly considered in this study, about 1.7 Sv of AL originate from the South Atlantic, possibly from mode water recirculation and from Drake Passage.

In the Cape Basin, we showed in Figures 6a and 7 that the source waters of AL are well mixed throughout the water column. On route, however, each individual component loses their original temperature and salinity characteristics at different locations due to mixing with ambient waters and/or surface fluxes. This occurs in the Arabian Sea for water from the Gulfs and in the larger Agulhas Current system for waters from the Gulfs and ITF (grey shading in Figure 9). However, water from south of Australia experiences very little modifications in properties during transit. The location and degree of mixing depend on the characteristics of the ambient waters such that the stronger the isopycnal gradient, the more potential for mixing (Figure 8). Therefore, the IO acts not only as a connector, but also as a modifier of water it receives from the Pacific and the marginal seas.

More profoundly Figure 9 shows that the IO exports 7.9 Sv from the Pacific to the Atlantic within 100 years. From a simple *Broeker* [1991] circulation point of view, this value therefore corresponds to the strength of the upper cell of the global conveyor belt. In other words, irrespective of the driving mechanisms, at least 7.9 Sv is the Pacific contribution to the so-called Atlantic warm-water route within this model. Due to the Lagrangian experiment design and in particular the duration of the integration, this value is given as a lower bound.

Of interest is to understand how an anomaly in properties in one of the sources would be communicated across the IO basin. For example, since the turn of the century, *Lee et al*. [2015] found an increase of about 0.2 PW in heat transport across the ITF (interannual heat transport difference 2003–2012), which also coincided with stronger through-flow, resulting from a prolonged negative phase of the Interdecadal Pacific Oscillation [*England et al*., 2014]. Our model simulates this increase as well. The question is whether (part of) this additional heat could be observed in the South Atlantic within the coming 1–2 decades? We found here that in the mean the IO cools and salinificates water coming from the ITF. Furthermore, based on our results, the efficiency at which the IO can communicate an anomaly across depends on the amplitude and duration of the anomaly, in addition to the characteristic of the ambient waters. In order to further address this question, sensitivity model experiments could be designed similar to *Lübbecke et al*. [2015] who assessed a warming signal transported across the South Atlantic from an increase in transport of Agulhas leakage.

Acknowledgments
The model data used for this study were kindly provided through collaboration within the DRAKKAR framework by the National Oceanographic Centre, Southampton, UK. We especially thank A.C. Coward and colleagues for making the data available. The Ariane-v2.2.6 Lagrangian package used can be obtained from http://www.univ-brest.fr/lpo/ariane/. Altimetry data for model validation were downloaded from http://aviso.oceanobs.com/. This work received funding from the Helmholtz Association and the GEOMAR Helmholtz Centre for Ocean Research Kiel (J.V.D., grant IV014/GH018), and the Cluster of Excellence "Future Ocean" (S.R., grant CP1412). The "Future Ocean" is funded within the framework of the Excellence Initiative by the Deutsche Forschungsgemeinschaft (DFG) on behalf of the German federal and state governments. The authors thank S. Lozier and C. Ummenhofer for helpful discussions of the results.

References

Al Saafani, M. A., S. S. C. Shenoi, D. Shankar, M. Aparna, J. Kurian, F. Durand, and P. N. Vinayachandran (2007), Westward movement of eddies into the Gulf of Aden from the Arabian Sea, *J. Geophys. Res.*, *112*, C11004, doi:10.1029/2006JC004020.

Beal, L. M., and K. A. Donohue (2013), The Great Whirl: Observations of its seasonal development and interannual variability, *J. Geophys. Res. Oceans*, *118*, 1–13, doi:10.1029/2012JC008198.

Beal, L. M., and S. Elipot (2016), Broadening not strengthening of the Agulhas Current since the early 1990s, *Nature*, *540*, 570–573, doi:10.1038/nature19853.

Beal, L. M., A. Ffield, and A. L. Gordon (2000), Spreading of Red Sea overflow waters since of the thickness influence, *J. Geophys. Res.*, *105*, 8549–8564.

Beal, L. M., T. K. Chereskin, Y. D. Lenn, and S. Elipot (2006), The sources and mixing characteristics of the Agulhas Current, *J. Phys. Oceanogr.*, *36*(11), 2060–2074, doi:10.1175/JPO2964.1.

Behera, S. K., et al. (2006), A CGCM study on the interaction between IOD and ENSO, *J. Clim.*, *19*(9), 1688–1705, doi:10.1175/JCLI3797.1.

Biastoch, A., J. R. E. Lutjeharms, C. W. Böning, and M. Scheinert (2008), Mesoscale perturbations control inter-ocean exchange south of Africa, *Geophys. Res. Lett.*, *35*, L20602, doi:10.1029/2008GL035132.

Biastoch, A., J. V Durgadoo, A. K. Morrison, E. van Sebille, W. Weijer, and S. M. Griffies (2015), Atlantic multi-decadal oscillation covaries with Agulhas leakage, *Nat. Commun.*, *6*, doi:10.1038/ncomms10082. [Available at https://www.nature.com/articles/ncomms10082.]

Blanke, B., and S. Raynaud (1997), Kinematics of the Pacific Equatorial Undercurrent: An Eulerian and Lagrangian approach from GCM results, *J. Phys. Oceanogr.*, *27*, 1038–1053, doi:10.1175/1520-0485(1997)027 < 1038:KOTPEU>2.0.CO;2.

Blanke, B., M. Arhan, G. Madec, and S. Roche (1999), Warm water paths in the equatorial atlantic as diagnosed with a general circulation model, *J. Phys. Oceanogr.*, *29*(11), 2753–2768, doi:10.1175/1520-0485(1999)029 < 2753:WWPITE>2.0.CO;2.

Bower, A. S., H. D. Hunt, and J. F. Price (2000), Character and dynamics of the Red Sea and Persian Gulf outflows, *J. Geophys. Res.*, *105*, 6387–6414.

Bower, A. S., D. M. Fratantoni, W. E. Johns, and H. Peters (2002), Gulf of Aden eddies and their impact on Red Sea Water, *Geophys. Res. Lett.*, *29*(21), 2025, doi:10.1029/2002GL015342.

Brodeau, L., B. Barnier, A.-M. Treguier, T. Penduff, and S. Gulev (2010), An ERA40-based atmospheric forcing for global ocean circulation models, *Ocean Modell.*, *31*(3), 88–104, doi:10.1016/j.ocemod.2009.10.005.

Broeker, W. (1991), The Great Ocean Conveyor, *Oceanography*, *4*(2), 79–89, doi:10.5670/oceanog.1991.07.

Chowdary, J. S., C. Gnanaseelan, B. Thompson, and P. S. Salvekar (2005), Water mass properties and transports in the Arabian Sea from Argo observations, *J. Atmos. Ocean Sci.*, *10*(3), 235–260, doi:10.1080/17417530600752825.

Döös, K., J. Nycander, and A. C. Coward (2008), Lagrangian decomposition of the Deacon Cell, *J. Geophys. Res.*, *113*, C07028, doi:10.1029/2007JC004351.

Durgadoo, J. V., B. R. Loveday, C. J. C. Reason, P. Penven, and A. Biastoch (2013), Agulhas leakage predominantly responds to the Southern Hemisphere Westerlies, *J. Phys. Oceanogr.*, *43*(10), 2113–2131, doi:10.1175/JPO-D-13-047.1.

Dussin, R., B. Barnier, and L. Brodeau (2014), The making of Drakkar forcing set DFS5, *DRAKKAR/MYOcean Rep. 05-10-14*, LGGE, Grenoble, France.

England, M. H., S. McGregor, P. Spence, G. A. Meehl, A. Timmermann, W. Cai, A. Sen Gupta, M. J. McPhaden, A. Purich, and A. Santoso (2014), Recent intensification of wind-driven circulation in the Pacific and the ongoing warming hiatus, *Nat. Clim. Change*, *4*(3), 222–227, doi:10.1038/nclimate2106.

Feng, M., C. Böning, A. Biastoch, E. Behrens, E. Weller, and Y. Masumoto (2011), The reversal of the multi-decadal trends of the equatorial Pacific easterly winds, and the Indonesian Throughflow and Leeuwin Current transports, *Geophys. Res. Lett.*, *38*, L11604, doi:10.1029/2011GL047291.

Fischer, J., F. Schott, and L. Stramma (1996), Currents and transports of the Great Whirl-Socotra Gyre system during the summer monsoon, August 1993, *J. Geophys. Res.*, *101*, 3573–3587.

Fratantoni, D. M., A. S. Bower, W. E. Johns, and H. Peters (2006), Somali Current rings in the eastern Gulf of Aden, *J. Geophys. Res.*, *111*, C09039, doi:10.1029/2005JC003338.

Gordon, A. L., S. Ma, D. B. Olson, P. Hacker, A. Ffield, L. D. Talley, D. Wilson, and M. Baringer (1997), Advection and diffusion of Indonesian Throughflow Water within the Indian Ocean South Equatorial Current, *Geophys. Res. Lett.*, *24*, 2573–2576.

Haines, M. A., R. A. Fine, M. E. Luther, and Z. Ji (1999), Particle trajectories in an Indian Ocean Model and sensitivity to seasonal forcing, *J. Phys. Oceanogr.*, *29*(4), 584–598, doi:10.1175/1520-0485(1999)029 < 0584:PTIAIO>2.0.CO;2.

Hallberg, R. (2013), Using a resolution function to regulate parameterizations of oceanic mesoscale eddy effects, *Ocean Modell.*, *72*, 92–103, doi:10.1016/j.ocemod.2013.08.007.

L'Hégaret, P., R. Duarte, X. Carton, C. Vic, D. Ciani, R. Baraille, and S. Corréard (2015), Mesoscale variability in the Arabian Sea from HYCOM model results and observations: Impact on the Persian Gulf Water path, *Ocean Sci.*, *11*(5), 667–693, doi:10.5194/os-11-667-2015.

Joseph, B., and P. S. Swathi (1999), Lagrangian particle transport in the Indian Ocean: A model study tank, *J. Geophys. Res.*, *104*, 5211–5224.

Jourdan, D., E. Balopoulos, M.-J. Garcia-Fernandez, and C. Maillard (1998), Objective analysis of temperature and salinity historical data set over the Mediterranean basin, in *IEEE Oceanic Engineering Society. OCEANS'98. Conference Proceedings (Cat. 98CH36259)*, vol. 1, pp. 82–87, IEEE. [Available at http://ieeexplore.ieee.org/stamp/stamp.jsp?arnumber=725649.]

Le Bars, D., H. A. Dijkstra, and W. P. M. De Ruijter (2013), Impact of the Indonesian Throughflow on Agulhas leakage, *Ocean Sci.*, *9*(5), 773–785, doi:10.5194/os-9-773-2013.

Lee, S.-K., W. Park, M. O. Baringer, A. L. Gordon, B. Huber, and Y. Liu (2015), Pacific origin of the abrupt increase in Indian Ocean heat content during the warming hiatus, *Nat. Geosci.*, *8*, 445–449, doi:10.1038/ngeo2438.

Legg, S., et al. (2009), Improving oceanic overflow representation in climate models: The Gravity Current Entrainment Climate Process Team, *Bull. Am. Meteorol. Soc.*, *90*(5), 657–670, doi:10.1175/2008BAMS2667.1.

Levitus, S., M. Conkright, T. P. Boyer, T. O'Brian, J. Antonov, C. Stephens, L. S. D. Johnson, R. Gelfeld (1998), World ocean database 1998, *Tech. Rep. NOAA Atlas NESDIS 18*, U.S. Gov. Print. Off., Washington, D. C.

Liu, Q.-Y., M. Feng, D. Wang, and S. Wijffels (2015), Interannual variability of the Indonesian Throughflow transport: A revisit based on 30 year expendable bathythermograph data, *J. Geophys. Res. Oceans*, *120*, 8270–8282, doi:10.1002/2015JC011351.

Lozier, M. S. (2010), Deconstructing the conveyor belt, *Science*, *328*(5985), 1507–1511, doi:10.1126/science.1189250.

Lübbecke, J. F., J. V. Durgadoo, and A. Biastoch (2015), Contribution of increased agulhas leakage to tropical Atlantic warming, *J. Clim.*, *28*(24), 9697–9706, doi:10.1175/JCLI-D-15-0258.1.

Lutjeharms, J. R. E. (2006), *The Agulhas Current*, Springer, Berlin Heidelberg.

Lutjeharms, J. R. E., and I. J. Ansorge (2001), The Agulhas Return Current, *J. Mar. Syst.*, *30*(1–2), 115–138, doi:10.1016/S0924-7963(01)00041-0.

Madec, G., and the NEMO team (2016), *NEMO ocean engine*, Note du Pôle de modélisation, Institut Pierre-Simon Laplace (IPSL), *27*, France. [Available at http://www.nemo-ocean.eu/About-NEMO/Reference-manuals.]

Meyers, G. (1996), Variation of Indonesian throughflow and the El Niño-Southern Oscillation, *J. Geophys. Res.*, *101*, 12,255–12,263.

Moat, B. I., et al. (2016), Major variations in subtropical North Atlantic heat transport at short (5 day) timescales and their causes, *J. Geophys. Res. Oceans*, *121*, 3237–3249, doi:10.1002/2016JC011660.

Nauw, J. J., H. M. van Aken, A. Webb, J. R. E. Lutjeharms, and W. P. M. de Ruijter (2008), Observations of the southern East Madagascar Current and undercurrent and countercurrent system, *J. Geophys. Res.*, *113*, C08006, doi:10.1029/2007JC004639.

Ou, H., and W. de Ruijter (1986), Separation of an inertial boundary current from a curved coastline., *J. Phys. Oceanogr.*, *16*, 280–289.

Prasad, T. G., M. Ikeda, and S. P. Kumar (2001), Seasonal spreading of the Persian Gulf Water mass in the Arabian Sea, *J. Geophys. Res.*, *106*, 17,059–17,071.

Qin, X., E. van Sebille, and A. Sen Gupta (2014), Quantification of errors induced by temporal resolution on Lagrangian particles in an eddy-resolving model, *Ocean Modell.*, *76*, 20–30, doi:10.1016/j.ocemod.2014.02.002.

Richardson, P. L. (2007), Agulhas leakage into the Atlantic estimated with subsurface floats and surface drifters, *Deep Sea Res., Part I*, *54*(8), 1361–1389, doi:10.1016/j.dsr.2007.04.010.

Richardson, P. L. (2008), On the history of meridional overturning circulation schematic diagrams, *Prog. Oceanogr.*, *76*(4), 466–486, doi:10.1016/j.pocean.2008.01.005.

Ridgway, K. R., and J. R. Dunn (2007), Observational evidence for a Southern Hemisphere oceanic supergyre, *Geophys. Res. Lett.*, *34*, L13612, doi:10.1029/2007GL030392.

Rimaud, J., S. Speich, B. Blanke, and N. Grima (2012), The exchange of Intermediate Water in the southeast Atlantic: Water mass transformations diagnosed from the Lagrangian analysis of a regional ocean model, *J. Geophys. Res.*, *117*, C08034, doi:10.1029/2012JC008059.

Rintoul, S. R., and S. Sokolov (2001), Baroclinic transport variability of the Antarctic Circumpolar Current south of Australia (WOCE repeat section SR3), *J. Geophys. Res.*, *106*, 2815–2832.

Roman, R. E., and J. R. E. Lutjeharms (2007), Red Sea Intermediate Water at the Agulhas Current termination, *Deep Sea Res., Part I*, *54*(8), 1329–1340, doi:10.1016/j.dsr.2007.04.009.

Rosell-Fieschi, M., S. R. Rintoul, J. Gourrion, and J. L. Pelegrí (2013), Tasman leakage of intermediate waters as inferred from Argo floats, *Geophys. Res. Lett.*, *40*, 5456–5460, doi:10.1002/2013GL057797.

Rühs, S., J. V. Durgadoo, E. Behrens, and A. Biastoch (2013), Advective timescales and pathways of Agulhas leakage, *Geophys. Res. Lett.*, *40*, 3997–4000, doi:10.1002/grl.50782.

Rusciano, E., S. Speich, and M. Ollitrault (2012), Interocean exchanges and the spreading of Antarctic Intermediate Water south of Africa, *J. Geophys. Res.*, *117*, C10010, doi:10.1029/2012JC008266.

Saji, N. H., B. N. Goswami, P. N. Vinayachandran, and T. Yamagata (1999), A dipole mode in the tropical Indian Ocean, *Nature*, *401*(6751), 360–363.

Sallée, J. B., N. Wienders, K. Speer, and R. Morrow (2006), Formation of subantarctic mode water in the southeastern Indian Ocean, *Ocean Dyn.*, *56*(5–6), 525–542, doi:10.1007/s10236-005-0054-x.

Schott, F. A., and J. Fischer (2000), Winter monsoon circulation of the northern Arabian Sea and Somali Current, *J. Geophys. Res.*, *105*, 6359–6376.
Schott, F. A., and J. P. McCreary (2001), The monsoon circulation of the Indian Ocean, *Prog. Oceanogr.*, *51*(1), 1–123, doi:10.1016/S0079-6611(01)00083-0.
Schott, F. A., S.-P. Xie, and J. P. McCreary (2009), Indian Ocean Circulation and climate variability, *Rev. Geophys.*, *47*, 1–46, doi:10.1029/2007RG000245.
Schulze, L. M. (2016), Freshwater fluxes and vertical mixing in the Labrador Sea, doctoral thesis, 198 pp., Univ. of Southampton, Ocean & Earth Sci., Southampton, U. K. [Available at http://eprints.soton.ac.uk/391105/.]
Sofianos, S. S., and W. E. Johns (2002), An Oceanic General Circulation Model (OGCM) investigation of the Red Sea circulation, 1. Exchange between the Red Sea and the Indian Ocean, *J. Geophys. Res.*, *107*(C11), 3196, doi:10.1029/2001JC001184.
Song, Q., A. L. Gordon, and M. Visbeck (2004), Spreading of the Indonesian Throughflow in the Indian Ocean*, *J. Phys. Oceanogr.*, *34*, 772–792, doi:10.1175/1520-0485(2004)034<0772:SOTITI>2.0.CO;2.
Speich, S., B. Blanke, P. de Vries, S. S. Drijfhout, K. Döös, A. Ganachaud, and R. Marsh (2002), Tasman leakage: A new route in the global ocean conveyor belt, *Geophys. Res. Lett.*, *29*(10), 1416, doi:10.1029/2001GL014586.
Speich, S., B. Blanke, and W. Cai (2007), Atlantic meridional overturning circulation and the Southern Hemisphere supergyre, *Geophys. Res. Lett.*, *34*, L23614, doi:10.1029/2007GL031583.
Sprintall, J., S. E. Wijffels, R. Molcard, and I. Jaya (2009), Direct estimates of the Indonesian Throughflow entering the Indian Ocean: 2004–2006, *J. Geophys. Res.*, *114*, C07001, doi:10.1029/2008JC005257.
Steele, M., R. Morfley, and W. Ermold (2001), PHC: A global ocean hydrography with high-quality Artic Ocean, *J. Clim.*, *14*, 2079–2087, doi:10.1175/1520-0442(2001)014 < 2079:PAGOHW>2.0.CO;2.
Stramma, L., and M. England (1999), On the water masses and mean circulation of the South Atlantic Ocean, *J. Geophys. Res.*, *104*, 20,863.
Swallow, J., M. Fieux, and F. Schott (1988), The boundary currents east and north of Madagascar: 1. Geostrophic currents and transports, *J. Geophys. Res.*, *93*, 4951.
Swallow, J. C., F. Schott, and M. Fieux (1991), Structure and transport of the East African Coastal Current, *J. Geophys. Res.*, *96*, 22,245.
The DRAKKAR Group (2007), Eddy-permitting ocean circulation hindcasts of past decades, in CLIVAR Exchanges, vol. 12, pp. 8–14. [Available at http://www.clivar.org/node/193.]
Tillinger, D., and A. L. Gordon (2009), Fifty years of the Indonesian Throughflow, *J. Clim.*, *22*(23), 6342–6355, doi:10.1175/2009JCLI2981.1.
Ullgren, J. E., H. M. van Aken, H. Ridderinkhof, and W. P. M. de Ruijter (2012), The hydrography of the Mozambique Channel from six years of continuous temperature, salinity, and velocity observations, *Deep Sea Res., Part I*, *69*, 36–50, doi:10.1016/j.dsr.2012.07.003.
Ummenhofer, C. C., F. U. Schwarzkopf, G. Meyers, E. Behrens, A. Biastoch, and C. W. Böning (2013), Pacific Ocean contribution to the asymmetry in Eastern Indian Ocean variability, *J. Clim.*, *26*(4), 1152–1171, doi:10.1175/JCLI-D-11-00673.1.
van Sebille, E., P. J. van Leeuwen, A. Biastoch, and W. P. M. De Ruijter (2010), On the fast decay of Agulhas rings, *J. Geophys. Res.*, *115*, C03010, doi:10.1029/2009JC005585.
van Sebille, E., L. M. Beal, and W. E. Johns (2011), Advective time scales of Agulhas leakage to the North Atlantic in surface drifter observations and the 3D OFES model, *J. Phys. Oceanogr.*, *41*(1947), 1026–1034, doi:10.1175/2011JPO4602.1.
van Sebille, E., M. H. England, J. D. Zika, and B. M. Sloyan (2012), Tasman leakage in a fine-resolution ocean model, *Geophys. Res. Lett.*, *39*, L06601, doi:10.1029/2012GL051004.
van Sebille, E., J. Sprintall, F. U. Schwarzkopf, A. Sen Gupta, A. Santoso, M. H. England, A. Biastoch, and C. W. Böning (2014), Pacific-to-Indian Ocean connectivity: Tasman leakage, Indonesian Throughflow, and the role of ENSO, *J. Geophys. Res. Oceans*, *119*, 1365–1382, doi:10.1002/2013JC009525.
Wijffels, S. E., G. Meyers, and J. Stuart Godfrey (2008), A 20-Yr average of the Indonesian Throughflow: Regional currents and the interbasin exchange, *J. Phys. Oceanogr.*, *38*, 1965–1978, doi:10.1175/2008JPO3987.1.
You, Y. (1998), Intermediate water circulation and ventilation of the Indian Ocean derived from water-mass contributions, *J. Mar. Res.*, *56*, 1029–1067, doi:10.1357/002224098765173455.
You, Y., and M. Tomczak (1993), Thermocline circulation and ventilation in the Indian Ocean derived from water mass analysis, *Deep Sea Res., Part I*, *40*(1), 13–56, doi:10.1016/0967-0637(93)90052-5.
You, Y., J. R. E. Lutjeharms, O. Boebel, and W. P. M. de Ruijter (2003), Quantification of the interocean exchange of intermediate water masses around southern Africa, *Deep Sea Res., Part II*, *50*(1), 197–228, doi:10.1016/S0967-0645(02)00384-3.